

Antarctic sea ice change based on a new sea ice dataset from 1992 to 2008

Li-Yin He^{1,2,3}, Chang-Qing Ke^{3,4,5,*}, Xiaobing Zhou⁶, Ya-Nan Cui¹, Liang Shan¹

¹School of Geographic and Oceanographic Sciences, Nanjing University, Nanjing 210023, PR China

²Division of Geological and Planetary Sciences, California Institute of Technology, 1200 East California Boulevard, Pasadena, CA 91125, USA

³Jiangsu Provincial Key Laboratory of Geographic Information Science and Technology, Nanjing University, Nanjing 210023, PR China

⁴Collaborative Innovation Center of South China Sea Studies, Nanjing University, Nanjing 210023, PR China

⁵Collaborative Innovation Center of Novel Software Technology and Industrialization, Nanjing University, Nanjing 210023, China

⁶Department of Geophysical Engineering, Montana Tech of The University of Montana, 1300 West Park Street, Butte, MT 59701, USA

ABSTRACT: The sea ice concentration dataset (covering the period 1992–2008) used in this study is a new dataset based on the Sea Ice Climate Change Initiative (SICCI) algorithm. We investigate whether the SICCI dataset is on a par with other datasets for studying sea ice cover changes in the Southern Ocean. We then examine spatiotemporal variations in sea ice derived from the SICCI dataset over the Southern Ocean, and analyse relationships of sea ice with sea surface temperature (SST). The results indicate that there is no significant difference between the SICCI dataset and the NASA Team dataset, and therefore the former can also be used for studying sea ice changes. Both sea ice extent (SIE) and sea ice area (SIA) derived from the SICCI dataset over the Southern Ocean increased slightly from 1992 to 2008, at rates of $(17.75 \pm 11.50) \times 10^3$ and $(17.37 \pm 9.51) \times 10^3 \text{ km}^2 \text{ yr}^{-1}$, respectively. Antarctic sea ice has significant seasonal variations; all seasonally averaged SIE and SIA show an increase, with spring showing the largest positive changing rate. The Weddell Sea, Ross Sea, and Indian Ocean have positive yearly changing rates in SIE and SIA, while the Bellingshausen/Amundsen seas and western Pacific Ocean have negative yearly changing rates. However, overall sea ice over the Southern Ocean has a slight positive trend, which is the same as the sea ice change pattern derived from the NASA Team dataset. This indicates that the contributions to the change in sea ice over the whole Southern Ocean due to the Weddell Sea, Ross Sea, and Indian Ocean dominate over those by the Bellingshausen/Amundsen seas and western Pacific Ocean. Further analysis shows that both SIE and SIA are negatively correlated with SST in the Southern Ocean or each of the 5 longitudinal sectors, and sea ice is more sensitive to SST in spring and autumn.

KEY WORDS: SICCI algorithm · Sea ice extent · Sea ice area · Sea surface temperature · Antarctica

— Resale or republication not permitted without written consent of the publisher —

1. INTRODUCTION

Antarctic sea ice is an important component of the global climate system, and it is expected to respond sensitively to climate change (Hanna 1996,

Pezza et al. 2012). The impact of Antarctic sea ice on climate is mainly due to its vast seasonal variation and positive feedback within the sea ice–seawater system (Comiso et al. 2011, Parkinson & Cavalieri 2012, Holland 2014). Sea ice on the ocean

surface increases surface albedo (Zhou et al. 2007), insulates ocean water from heat loss or gain, and provides a barrier to the exchange of momentum (e.g. wind) and mass (e.g. water vapour and CO₂) between the ocean and atmosphere (Vaughan et al. 2013). The existence of sea ice influences atmospheric and oceanic circulation in the Southern Hemisphere (Raphael et al. 2011). Regional climate changes affect sea ice characteristics, and these changes in the Southern Ocean can feed back to the climate system, both regionally and globally (Yuan & Martinson 2000, Goosse & Zunz 2014).

Regional sea ice observations have revealed significant interannual changes in sea ice coverage in the Southern Ocean (Walsh & Chapman 2001). It is difficult to investigate Antarctic sea ice characteristics that vary with time, due to its vastness and the harsh conditions of the polar environment. Satellite remote sensing has provided a reliable tool for continuously monitoring changes in sea ice cover since the 1960s (Cavalieri et al. 2003, Gallaher et al. 2014). Satellite passive microwave (PM) sea ice concentration products based on Special Sensor Microwave/Imager (SSM/I), Special Sensor Microwave Imager/Sounder (SSMIS), and Advanced Microwave Scanning Radiometer for the Earth Observing System (AMSR-E) measurements are normally used to analyse Antarctic sea ice change (Worby & Comiso 2004, Comiso & Nishio 2008, Spreen et al. 2008, Parkinson & Cavalieri 2012, Raphael & Hobbs 2014, Shao & Ke 2015).

Several algorithms have been developed to convert the observed microwave brightness temperature (T_b) to sea ice concentration (SIC). These algorithms include the NASA Team (NT) algorithm (Cavalieri et al. 1984), the Bootstrap frequency mode (BF) algorithm (Comiso 1986), the Bristol (BR) algorithm (Smith 1996), the Arctic Radiation and Turbulence Interaction Study (ARTIST) Sea Ice (ASI) algorithm (Kaleschke et al. 2001), the European Organisation for the Exploitation of Meteorological Satellites' (EUMETSAT's) Ocean and Sea Ice Satellite Application Facility (OSISAF) algorithm (Eastwood 2012), and the European Space Agency (ESA) Sea Ice Climate Change Initiative (SICCI) algorithm (Ivanova et al. 2015). Sea ice extent (SIE, defined as the summed areas of all grid cells in the region of interest having ≥15% SIC) and sea ice area (SIA, defined as the sum of the products of ice concentration and area for each grid cell within the region of interest) can then be calculated based on SIC.

In contrast to the Arctic, where a significant decrease since 1979 has been observed (Cavalieri & Par-

kinson 2012), SIE was observed to increase slightly in the Southern Ocean in the past decades (Comiso & Nishio 2008, Parkinson & Cavalieri 2012). PM SIE data based on the NT algorithm indicated a significant positive trend of $(15.3 \pm 3.9) \times 10^3 \text{ km}^2 \text{ yr}^{-1}$ for the period between 1979 and 2013 (Simmonds 2015). There are large regional differences in the change of Antarctic sea ice. Much of the increase has occurred in the Ross Sea and less so in the Weddell Sea and Indian Ocean (Fig. 1). However, the Bellingshausen/Amundsen seas show a significant decrease in sea ice coverage (Parkinson & Cavalieri 2012). In the northeast and west Antarctic Peninsula and southern Bellingshausen Sea region, later ice advance, earlier retreat, and shorter ice cover duration occurred over the period 1979/1980–2010/2011 (Stammerjohn et al. 2012). In contrast, in the western Ross Sea region, sea ice retreated and advanced by >1 mo later and earlier, respectively, resulting in a shorter ice-free summer season by >2 mo (Stammerjohn et al. 2012). Simpkins et al. (2013) reported a similar observation on the duration of Antarctic sea ice.

The SICCI algorithm is a new hybrid algorithm constructed as a weighted combination of the BF algorithm and the BR algorithm (Smith 1996), with a dynamic tie-points approach to achieve good performance over areas with both thick and thin ice (Ivanova et al. 2015). A new dataset available over 1992–2008 is produced by the algorithm. It is shorter than existing datasets, but offers opportunity to study Antarctic sea ice change, and it will be extended in the future. Uncertainty exists in SIE estimated from remotely sensed data. Intercomparison between different datasets may help to understand this uncertainty. Some studies have shown that Antarctic sea ice variability is related to sea surface temperature (SST) (Vaughan et al. 2003, Comiso 2010). Further investigation on the cause of Antarctic sea ice variability is important for the study of the Antarctic sea ice process. The objectives of this study are twofold. (1) We will intercompare the SICCI sea ice cover, SIA, and SIE derived with this new algorithm with other algorithms to identify potential differences, advantages, and disadvantages of the new dataset when investigating changes and trends of Antarctic sea ice cover. (2) We will examine spatiotemporal variations in sea ice derived from the SICCI dataset over the Southern Ocean (and analyse possible mechanisms that could lead to sea ice changes), and correlate SIE with SST to examine the impacts of production and melt on sea ice change resulting from SST variations.

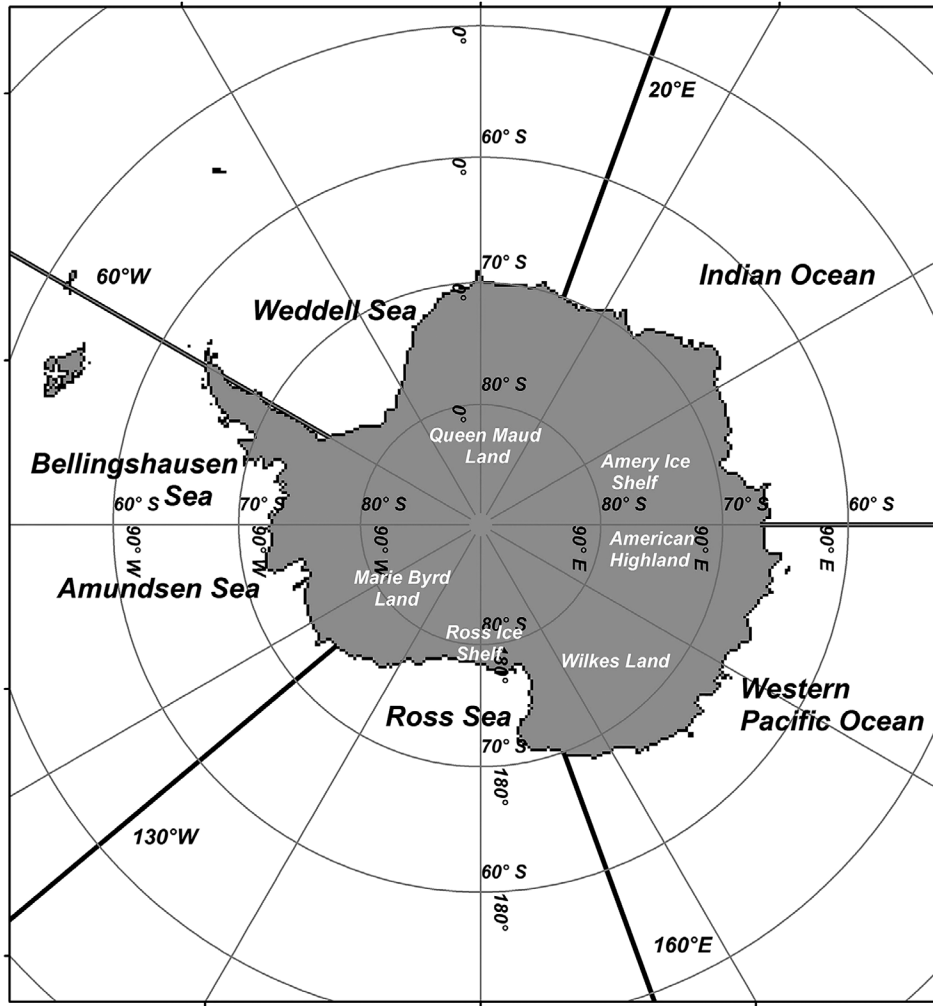


Fig. 1. Southern Ocean, including identification of the 5 longitudinal sectors used for sea ice analyses

2. DATA AND METHODS

2.1. SICCI algorithm and dataset

SIC has been retrieved from satellite microwave radiometers for over 30 yr. The SSM/Is on board F10, F11, F13, F14, and F15 satellites of the Defense Meteorological Satellite Program (DMSP) collected data on a daily basis since 7 January 1991. These satellites circled the Earth in a sun-synchronous, near-circular polar orbit. The instrument is a multichannel PM radiometer scanning the ground scene at a constant angle of about 53° incidence angle, and a complete coverage of the polar regions is achieved in 1 d (Hollinger et al. 1987). The SSM/Is record Tbs with imaging channels that are relevant to the SIC retrievals, namely, the 19 GHz, 37 GHz, and 85 GHz imaging channels.

The majority of sea ice algorithms are based on the radiative transfer equation (Svendsen et al. 1983). Many algorithms have been developed to convert observed microwave Tbs to SIC, and several typical algorithms are shown in Table 1. We will focus on the algorithms listed in Table 1. The NT algorithm uses the polarisation ratio

$$PR = \frac{Tb(19V) - Tb(19H)}{Tb(19V) + Tb(19H)} \quad (1)$$

at 19 GHz, where V is vertical polarization, H is horizontal polarization; and gradient ratios (GR)

$$GR = \frac{Tb(37V) - Tb(19H)}{Tb(37V) + Tb(19V)} \quad (2)$$

at 19 and 37 GHz to retrieve SIC (Cavaliere et al. 1984, Comiso et al. 1997), and it is also one of the earliest sea ice algorithms. The BF algorithm (Comiso

Table 1. Sea ice concentration algorithms mentioned in this study (adapted from Ivanova et al. 2015). **P** indicates that the algorithm is based on the polarisation difference or ratio at a single frequency; **F** indicates that the algorithm uses 2 different frequencies at the same polarisation (i.e. a spectral gradient). The names of the high-frequency algorithms (and the algorithms partially using high frequencies) are shown in **bold**, while the rest are low-frequency algorithms. Bootstrap F: Bootstrap frequency; OSISAF: Ocean and Sea Ice Satellite Application Facility; SICCI: Sea Ice Climate Change Initiative

Algorithm	Reference	Channels
NASA Team	Cavalieri et al. (1984)	19V, 19H, 37V PF
Bootstrap F	Comiso (1986)	37V, 37H P
Bristol	Smith (1996)	19V, 37V, 37H PF
OSISAF	Eastwood (2012)	19V, 37V, 37H PF
SICCI	Ivanova et al. (2015)	19V, 37V, 37H P

1986) works in the frequency mode for discriminating atmosphere and ocean (roughness) effects on the open water from low-concentration ice, as well as for discriminating Tb variations because of changes in snow cover and other surface effects in consolidated ice areas from actual variations in concentration. The BF algorithm is only used in the Antarctic, but a combination of both the BF and polarisation modes is used in the Arctic (Comiso et al. 1997). As a result of ice layers in the snow cover and discontinuous ice concentrations, significantly different SICs estimated by the BF and NT are found. The BR algorithm (Smith 1996) uses 3-dimensional scatter plots and introduces transformed coordinates to overcome these problems. The OSISAF algorithm is a weighted combination of the BF and BR; therefore, it is a hybrid algorithm, where the BF is expected to have low sensitivity to atmospheric effects over open water, and the BR is expected to have better performance over ice (Eastwood 2012).

The SICCI algorithm is based on 3 PM radiometer channels, near 19 GHz (vertical polarisation) and 37 GHz (both vertical and horizontal polarisations), and it is a slightly modified version of the OSISAF algorithm, designed to achieve better performance over areas with thin ice (Ivanova et al. 2015). Similar to the OSISAF algorithm, the SICCI algorithm is constructed as a weighted combination of the BF and BR algorithms. The BR algorithm estimates dominate at the high-concentration range, while the BF algorithm is given more weights at the low-concentration range. To take advantage of the good performance of the BF and BR algorithm for thin ice, the algorithm and weights are applied as given in Eq. (3), below, this subsection. Different weights are tested on the

thin ice dataset. The optimal values are chosen so that the hybrid algorithm performs better over thin ice and at the same time keeps its performance under other conditions at the same level as the original OSISAF algorithm. In particular, values of 0 and 40% in the original OSISAF algorithm are used. The equation is as follows:

$$\text{SIC} = c_{\text{BF}} \times w_{\text{BF}} + c_{\text{BR}} \times w_{\text{BR}} \quad (3)$$

where c_{BF} and w_{BF} are SIC and weight, respectively, for SIC from the BF; and c_{BR} and w_{BR} are SIC and weight, respectively, for SIC from the BR. For $c_{\text{BF}} < 70\%$, as obtained by the BF, weight is $w_{\text{BF}} = 1$; for high values ($c_{\text{BF}} \geq 90\%$), it is $w_{\text{BF}} = 0$. For values between 70 and 90%, weight for the BF is defined as $w_{\text{BF}} = 1.0 - (c_{\text{BF}} - 0.7)/0.2$. Weight for the BR (w_{BR}) is $1.0 - w_{\text{BF}}$.

An individual tie-point for each surface type (open water, first-year ice, and multiyear ice for the SICCI algorithm) is selected using the NT algorithm. The tie-points to the SICCI algorithm are adapted dynamically to the sensor data and vary every day as a running average of Tb over a -7 to $+7$ d window (a running average of Tb over a -15 to $+15$ d window is used in the OSISAF data record). Moreover, the tie-point for open water is selected in a buffer region at the outer limit of a monthly varying air temperature, to ensure that these open water signatures are representative under the typical weather conditions prevailing in the vicinity of the ice edge. Being derived separately for each sensor and platform, the dynamic tie-points method compensates for intersensor differences in a consistent manner. Compared with the OSISAF algorithm, the dynamic tie-points approach of the SICCI algorithm has a clear advantage in adapting better to seasonal and interannual variations of sea ice emissivity, and dynamic tie-points serve to ensure that the algorithm gives 0% SIC for areas of open water and 100% SIC for areas of consolidated ice across all seasons and across the PM sensors used.

In the SICCI processing chain, European Centre for Medium-Range Weather Forecasting (ECMWF) ERA-Interim (ECMWF Re-Analysis, ERA) data, including fields of 10 m wind speed, total columnar water vapour, and temperature at 2 m, and a radiative transfer model (RTM) (Andersen et al. 2006) are used to correct the Tbs because of atmospheric effects. The tie-points are then estimated from the corrected Tbs. Finally, these tie-points along with the corrected Tbs are used to retrieve SIC.

The SICCI algorithm with dynamic tie-points and atmospheric correction could be a good choice for

SIC climate dataset retrievals. Errors of the retrieved SIC data using the SICCI algorithm are estimated by an uncertainty model, and are included into the dataset (Ivanova et al. 2015). Because of the coarse resolution of the radiometers, the data may be influenced by land up to 50 km from the coastline. The emissivity of land along the coastline is similar to sea ice emissivity, and is much higher than water emissivity. This means that in the coastal zone, if there is open water or intermediate concentrations, sea ice concentration will be overestimated. To reduce this overestimation, ice concentration near the coast is filtered using a statistical method, which was described in Cavalieri et al. (1999). The missing data, which occur in several forms, such as missing scan lines and missing orbits, are interpolated by ice concentration estimates from the previous and next daily products to fill the data gaps (Ivanova et al. 2015). We obtained the SICCI SIC data from the Integrated Climate Data Centre (ICDC, <http://icdc.zmaw.de>), Hamburg University, Germany.

Although SSM/I F13 continues operations after 31 December 2008, the current SICCI dataset based on the SSM/I stops on this date. Therefore, we use the daily SICCI dataset for the period January 1992–December 2008, with a grid cell size of 25×25 km. The mean SIC of a month can be calculated only if there are at least 14 daily valid SICs in that month; thus, a monthly time series of Antarctic SICs from 1992 to 2008 is established. The monthly SIC data are used to calculate seasonal and yearly averages and then are used to calculate SIE and SIA.

2.2. SST

Optimum Interpolation Version 2 Sea Surface Temperature (OI.V2 SST) is provided by the Ocean, Atmosphere and Geoscience Laboratory of NOAA. The dataset contains a time series of weekly and monthly mean SSTs with a $1^\circ \times 1^\circ$ resolution (Reynolds et al. 2002). We reproject the monthly SST data so that they have the same polar projection as the SICCI data; then, we resample the monthly SST data so that they have the same spatial resolution as the SIC data with 25×25 km. Then, we calculate the monthly mean SST of pixels of which the corresponding SICs are $>15\%$ for 5 longitudinal sectors (Fig. 1) and the Southern Ocean, and establish the corresponding monthly SST time series. The monthly SST data from 1992 to 2008 are compared to Antarctic SIC data to investigate potential SST–sea ice cover change interactions.

2.3. Methods

As in previous studies such as Parkinson & Cavalieri (2012), the Southern Ocean around Antarctica is divided into 5 longitudinal sectors: western Pacific Ocean (90° – 160° E), Ross Sea (160° E– 130° W), Bellingshausen and Amundsen seas (130° – 60° W), Weddell Sea (60° W– 20° E, plus the small ocean area between the east coast of the Antarctic Peninsula and 60° W), and Indian Ocean (20° – 90° E) (Fig. 1). The austral seasons are used in this paper, i.e. spring (October, November, and December), summer (January, February, and March), autumn (April, May, and June), and winter (July, August, and September).

To obtain monthly changing rates, the seasonal trend is removed by creating monthly deviations, which are calculated by subtracting from each individual monthly average the 17 yr average for that month. This is done following the procedure in Parkinson & Cavalieri (2012) and subsequent works. Linear fittings of the monthly, seasonal, and yearly SIE and SIA data using the least square root method for the Southern Ocean and the 5 longitudinal sectors are performed. Standard deviations of the slopes of these linear fittings are then calculated, and whether the changing rates are statistically significant is roughly determined by the ratio R of the changing rate to its standard deviation (Taylor 1997). This is essentially the same as using the Student's t -test with 15 degrees of freedom (2 fewer than the number of data points). The correlation coefficients between the time series of the yearly and seasonal SIA, SIE, and SST are calculated, and respective significance levels are estimated. Final results are presented for the entire Southern Ocean and the 5 longitudinal sectors.

3. RESULTS AND DISCUSSION

3.1. Comparisons between the SICCI and NT datasets

The monthly mean SICCI SIC data coincide well with the NT SIC data when SIC is $>68\%$ (mostly occurs in winter), while they have a little bias when SIC is $<68\%$ (mostly in summer) (Fig. 2a). However, all algorithms have errors in summer because sea ice melting and quick change result in microwave signal noise. R^2 (0.94) is high; therefore, the bias is acceptable. Overall, the monthly mean SICCI SIC data are consistent with the NT SIC data over the

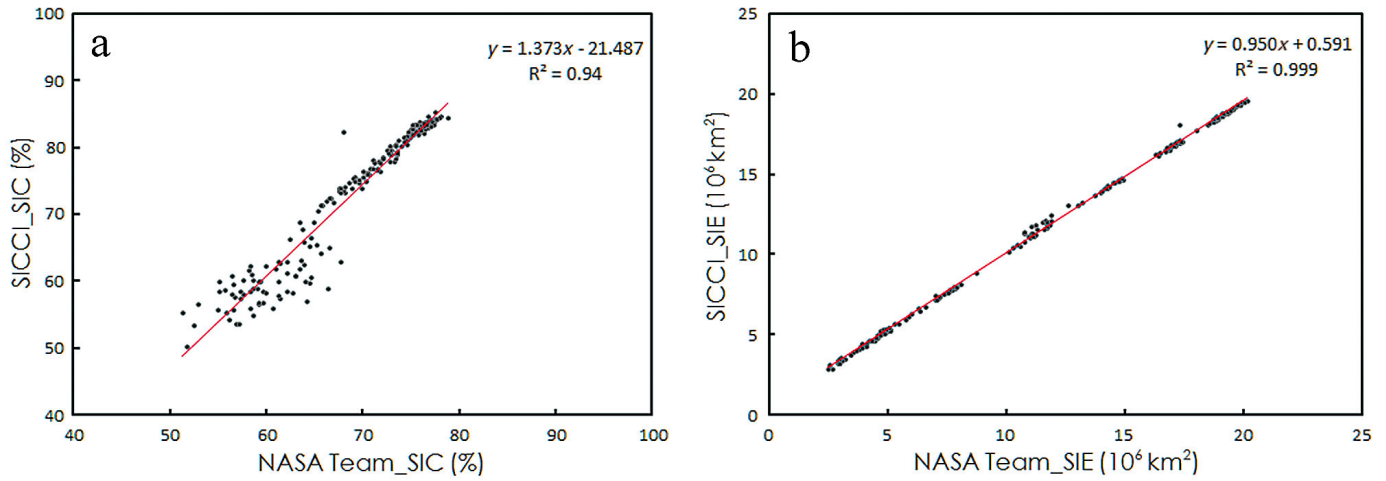


Fig. 2. Comparisons between the Sea Ice Climate Change Initiative (SICCI) dataset and NASA Team dataset over the Southern Ocean from 1992 to 2008. (a) Monthly sea ice concentration (SIC) and (b) monthly sea ice extent (SIE)

Southern Ocean from 1992 to 2008. The monthly mean SICCI SIE data agree perfectly well ($R^2 = 0.999$) with the NT SIE data in either winter (large SIE) or summer (small SIE) (Fig. 2b). All these indicate that the SICCI dataset over the Southern Ocean from 1992 to 2008 is on a par with the NT dataset; that is, they are not significantly different from each other. We will thus use the SICCI dataset for studying sea ice changes.

3.2. SIE

3.2.1. Southern Ocean

On average, September is typically the month of maximum sea ice coverage, and February is typically the month of minimum sea ice coverage following the austral melting season; most of the remaining sea ice in February is found in the region to the east of the

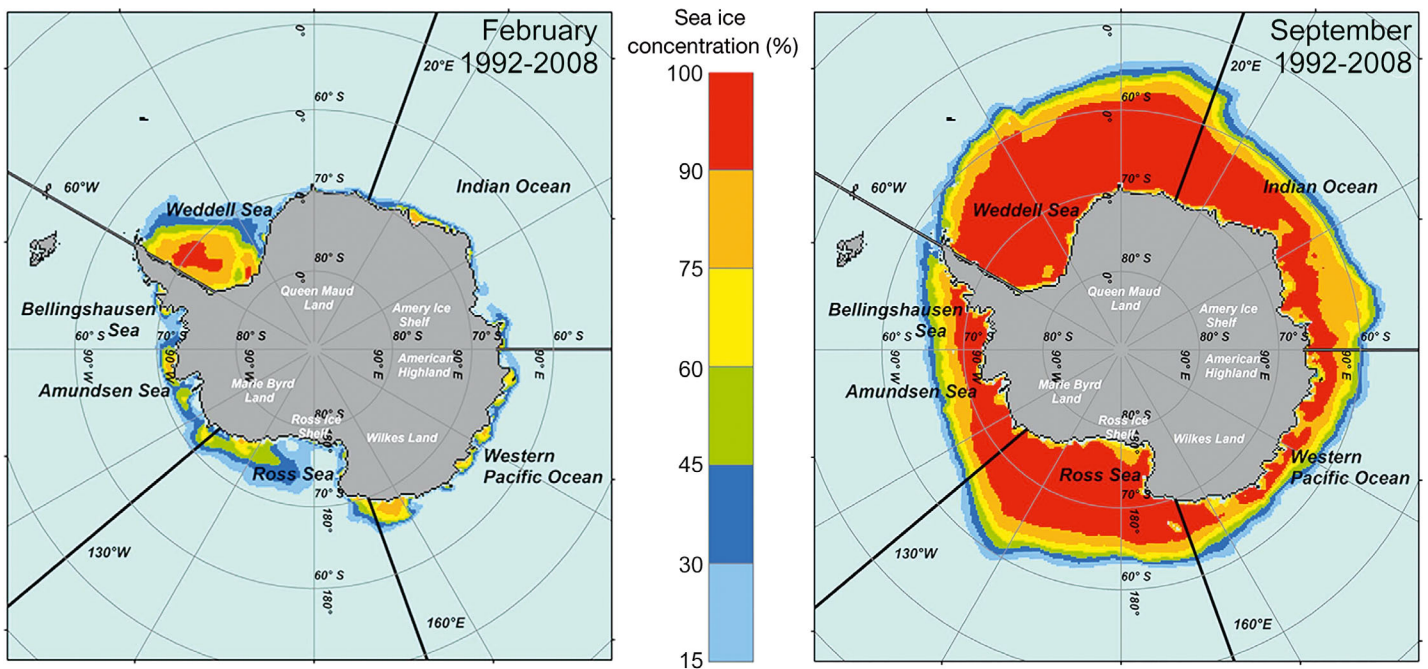


Fig. 3. Southern Ocean February and September sea ice concentrations, averaged over the years 1992–2008, as derived from Special Sensor Microwave/Imager satellite observations

Table 2. Average sea ice extent (SIE) and sea ice area (SIA) for yearly, February, and September data in the Southern Ocean and in each of the 5 longitudinal sectors delineated in Fig. 1 for the period 1992–2008. SO: Southern Ocean; WS: Weddell Sea; RS: Ross Sea; IO: Indian Ocean; BS: Bellingshausen and Amundsen seas; PO: western Pacific Ocean

	Yearly ($\times 10^6 \text{ km}^2$)	February ($\times 10^6 \text{ km}^2$)	September ($\times 10^6 \text{ km}^2$)
SIE			
SO	12.39	3.54	19.11
WS	4.54	1.42	6.80
RS	3.06	0.87	4.29
IO	2.06	0.29	3.76
BS	1.42	0.51	2.23
PO	1.31	0.46	2.03
SIA			
SO	9.56	2.05	15.99
WS	3.69	1.00	5.98
RS	2.43	0.43	3.69
IO	1.51	0.12	3.10
BS	1.02	0.25	1.71
PO	0.91	0.25	1.51

Antarctic Peninsula (Fig. 3). Mean SIEs in the Southern Ocean in September and February are 19.11×10^6 and $3.54 \times 10^6 \text{ km}^2$, respectively, over the 17 yr period (Table 2). The monthly averages of SIEs (Fig. 4a) show a moderate interannual variability, which is different from the much greater interannual variability within the 5 longitudinal sectors (Figs. S1–S5 in the Supplement, www.int-res.com/articles/suppl/c071p155_supp.pdf). The September SIEs range from a minimum of $18.49 \times 10^6 \text{ km}^2$ in 2002 to a maximum of $19.62 \times 10^6 \text{ km}^2$ in 2006. The maximum in 2006 was also observed by Parkinson & Cavalieri (2012) for the period 1979–2010. The February SIEs range from a minimum of $2.86 \times 10^6 \text{ km}^2$ in 1997 to a maximum of $4.43 \times 10^6 \text{ km}^2$ in 2008. The monthly SIE deviation shows that an increasing rate exists, with a positive slope of $(17.69 \pm 6.18) \times 10^3 \text{ km}^2 \text{ yr}^{-1}$ for the period between 1992 and 2008 (Fig. 4b).

The yearly and seasonally averaged SIEs all show positive changing rates in the Southern Ocean (Fig. 4c, Table 3), and the yearly changing rate in SIE is $(17.75 \pm 11.50) \times 10^3 \text{ km}^2 \text{ yr}^{-1}$. On a seasonal basis, spring shows the largest positive changing rate of $(35.29 \pm 10.81) \times 10^3 \text{ km}^2 \text{ yr}^{-1}$, followed by the changing rate in summer. The relative changing rates in summer and winter are approximately one-half and one-fifth, respectively, of that in spring. The largest relative change in the seasonal mean SIE, given in percent per decade, is observed for summer: 4.29 ± 6.38 .

3.2.2. Five longitudinal sectors

The Weddell Sea is the largest in area among the 5 longitudinal sectors and also has the largest sea ice cover, with a mean SIE of $4.54 \times 10^6 \text{ km}^2$, and the Ross Sea has a smaller SIE than the Weddell Sea. Mean SIEs then decrease in order from the Indian Ocean to the Bellingshausen/Amundsen seas to the western Pacific Ocean (Table 2). The Weddell Sea has the largest magnitude of variation in monthly SIE, ranging from $0.97 \times 10^6 \text{ km}^2$ in February 1999 to $7.42 \times 10^6 \text{ km}^2$ in August 1992, followed by the Ross Sea, Indian Ocean, Bellingshausen/Amundsen seas, and the western Pacific Ocean, which has the lowest SIE (Figs. S1a–S5a in the Supplement). The phasings of the annual cycle of SIE in the Weddell Sea, Ross Sea, Bellingshausen/Amundsen seas, and western Pacific Ocean (insets of Figs. S1a, S2a, S4a, S5a) are similar to that of the Southern Ocean. However, annual SIE in the Indian Ocean has a peak value occurring in October rather than September (but only slightly greater than the average September value), which is different from those in the other sectors (Fig. S3a inset). The Weddell Sea, Ross Sea, and Indian Ocean have a positive interannual trend in monthly SIE deviations during the period 1992–2008, and the Ross Sea has the highest one, with a slope of $(16.62 \pm 3.94) \times 10^3 \text{ km}^2 \text{ yr}^{-1}$, which is slightly smaller than that of the Southern Ocean but much greater than that of the Weddell Sea (Figs. S1b–S3b). The Bellingshausen/Amundsen seas and western Pacific Ocean have negative interannual trends in monthly SIE deviations (Figs. S4b & S5b).

Among the 5 longitudinal sectors, the Weddell Sea, Ross Sea, and Indian Ocean have positive yearly changing rates, and the Ross Sea has the highest one (Table 3). This indicates that sea ice cover in the 3 sectors increased from 1992 to 2008, and the Ross Sea experienced the largest increase (Figs. S1c–S3c). The yearly changing rate of SIE in the Indian Ocean is about half as much as that in the Ross Sea, and that $(2.05 \times 10^3 \text{ km}^2 \text{ yr}^{-1})$ in the Weddell Sea is quite close to zero. In contrast, the Bellingshausen/Amundsen seas and western Pacific Ocean have negative yearly changing rates (Figs. S4c & S5c); that of the former is higher, and sea ice decreased more evidently. The largest relative change in the yearly changing rate of SIE is observed in the Ross Sea: $6.14 \pm 3.86\%$ decade⁻¹ (Table 3). Seasonal changing rates are different and very complicated for each season among the 5 longitudinal sectors (Table 3). Seasonal changing rates in SIE in the Ross Sea are positive in all seasons, and the largest rate, $(24.13 \pm 10.18) \times 10^3 \text{ km}^2 \text{ yr}^{-1}$,

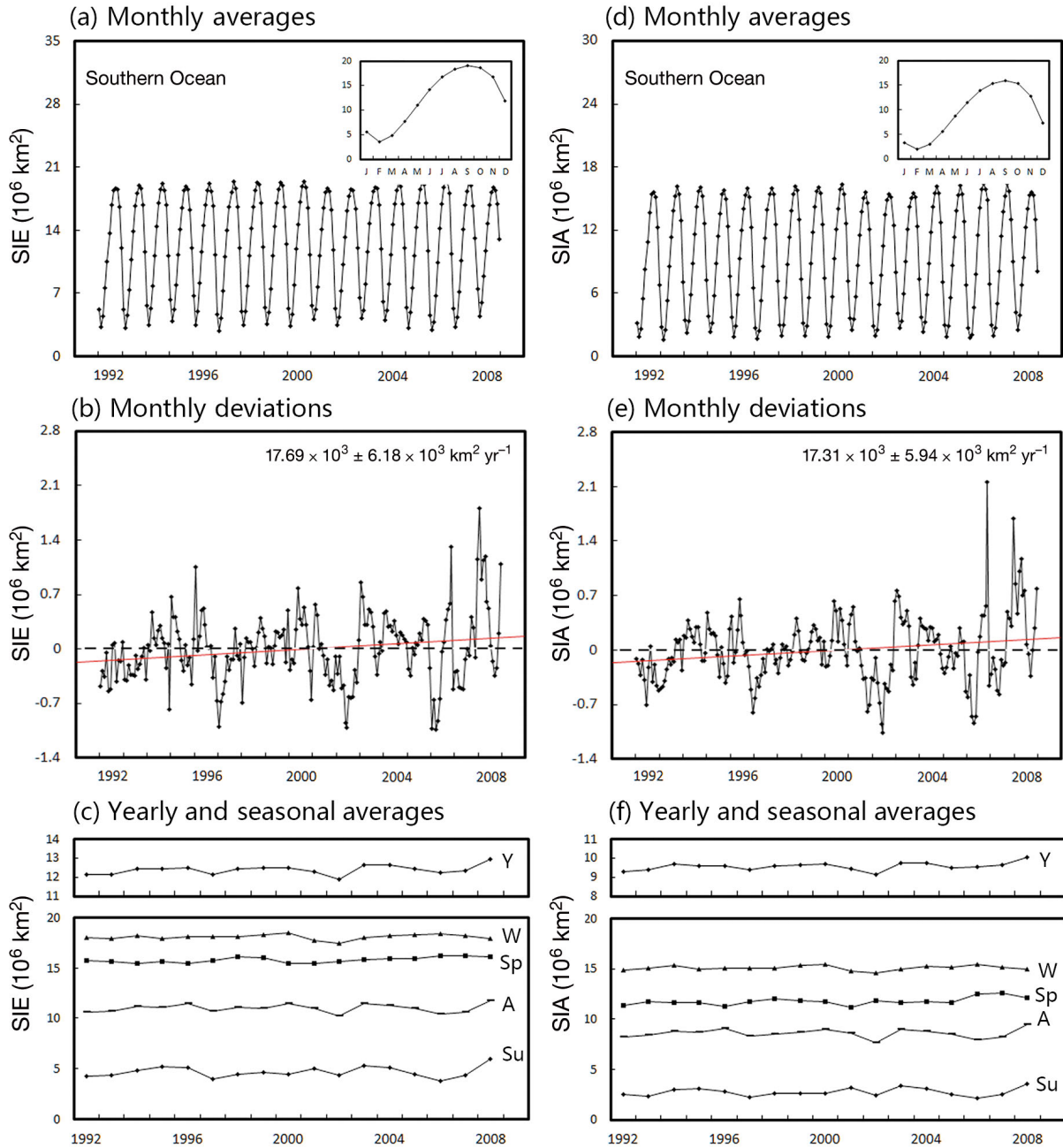


Fig. 4. Time series of monthly averages of sea ice extent (SIE) and sea ice area (SIA) for the Southern Ocean from January 1992 through December 2008, respectively, with insets showing the average annual cycle, calculated from (a,d) Special Sensor Microwave/Imager satellite data; (b,e) monthly deviations of SIE and SIA, respectively (data in top-right: slope \pm SE); and (c,f) yearly and seasonal averages of SIEs and SIAs, respectively. Y: yearly averages; Su: summer averages (January–March); A: autumn averages (April–June); W: winter averages (July–September); Sp: spring averages (October–December)

occurs in autumn. Seasonal changing rates in SIE in the Indian Ocean are positive; however, those in the Bellingshausen/Amundsen seas are negative (Table 3). The largest relative trends in summer occur in the Ross Sea and Indian Ocean (close to 20% decade⁻¹), and those in autumn occur in the Ross Sea and Bellingshausen/Amundsen seas (close to +10

and -10% decade⁻¹, respectively). Overall, these results demonstrate that sea ice cover in the Ross Sea and Indian Ocean increased during the 17 yr period (Figs. S2c & S3c) and had an important contribution to the overall increase in sea ice over the Southern Ocean due to their positive yearly changing rate, especially in the Ross Sea (Comiso et al. 2011).

Table 3. Changing rates (\pm SD) of the yearly and seasonal sea ice extents (SIEs) in the Southern Ocean as a whole and in each of the 5 longitudinal sectors delineated in Fig. 1 for the period 1992–2008. R is the ratio of the magnitude of the slope to the SD; in the R column, **bold** indicates statistical significance of $\geq 95\%$. SO: Southern Ocean; WS: Weddell Sea; RS: Ross Sea; IO: Indian Ocean; BS: Bellingshausen and Amundsen seas; PO: western Pacific Ocean

	SIE		R
	($10^3 \text{ km}^2 \text{ yr}^{-1}$)	(% decade $^{-1}$)	
Yearly			
SO	17.75 \pm 11.50	1.46 \pm 0.95	1.54
WS	2.05 \pm 11.95	0.42 \pm 2.43	0.17
RS	16.68 \pm 10.49	6.14 \pm 3.86	1.59
IO	8.98 \pm 4.99	4.52 \pm 2.51	1.80
BS	-8.45 \pm 10.65	-5.48 \pm 6.91	-0.79
PO	-2.93 \pm 3.94	-2.31 \pm 3.10	-0.74
Spring			
SO	35.29 \pm 10.81	2.24 \pm 0.69	3.26
WS	16.64 \pm 13.92	2.81 \pm 2.35	1.20
RS	14.18 \pm 14.47	3.89 \pm 3.97	0.98
IO	12.17 \pm 9.89	3.81 \pm 3.10	1.23
BS	-7.02 \pm 5.22	-5.51 \pm 4.10	-1.34
PO	0.76 \pm 5.58	0.53 \pm 3.89	0.14
Summer			
SO	18.42 \pm 27.38	4.29 \pm 6.38	0.67
WS	2.31 \pm 19.69	1.11 \pm 9.49	0.12
RS	14.51 \pm 14.85	17.29 \pm 17.70	0.98
IO	6.06 \pm 4.43	19.36 \pm 14.16	1.37
BS	-2.37 \pm 5.58	-4.81 \pm 11.32	-0.42
PO	-2.08 \pm 4.49	-3.63 \pm 7.83	-0.46
Autumn			
SO	10.03 \pm 21.02	0.94 \pm 1.98	0.48
WS	-4.00 \pm 19.40	-0.90 \pm 4.36	-0.21
RS	24.13 \pm 10.18	9.58 \pm 4.04	2.37
IO	5.99 \pm 6.86	4.63 \pm 5.30	0.87
BS	-10.49 \pm 9.29	-8.76 \pm 7.75	-1.13
PO	-5.60 \pm 5.59	-4.69 \pm 4.68	-1.00
Winter			
SO	7.27 \pm 12.51	0.40 \pm 0.70	0.58
WS	-6.75 \pm 13.32	-0.93 \pm 1.85	-0.51
RS	13.89 \pm 12.88	3.60 \pm 3.33	1.08
IO	11.70 \pm 10.50	3.71 \pm 3.33	1.11
BS	-6.77 \pm 8.88	-3.63 \pm 4.76	-0.76
PO	-4.80 \pm 7.53	-2.55 \pm 4.00	-0.64

3.3. SIA

3.3.1. Southern Ocean

SIA varies in time in a similar pattern as SIE (Fig. 4 & Figs. S1–S5). SIA minima (February) and maxima (September) are 2.05×10^6 and $15.99 \times 10^6 \text{ km}^2$, respectively (Table 2, Fig. 4d inset). SIA monthly averages in the Southern Ocean show a similar seasonal changing pattern as SIE monthly averages (Fig. 4d) but with smaller magnitudes. The monthly deviation changing rate of SIA also shows the same basic seasonal cycle as that of SIE (Fig. 4e). The yearly SIA

changing rate for the Southern Ocean is $(17.37 \pm 9.51) \times 10^3 \text{ km}^2 \text{ yr}^{-1}$ (Table 4); this indicates that like SIE, SIA in the Southern Ocean increased from 1992 to 2008.

The changing rate in SIA in the Southern Ocean is also positive in each season, with the highest magnitude occurring in spring at $(43.54 \pm 15.57) \times 10^3 \text{ km}^2 \text{ yr}^{-1}$ (Table 4). The lowest magnitude of the seasonal changing rate in SIA occurs in winter, which is same as SIE (Fig. 4f). Furthermore, for autumn, winter, and summer, the changing rates in SIA have lower magnitudes than those in SIE, whereas in spring the changing rate in SIA has a slightly higher magnitude than the changing rate in SIE (Tables 3 & 4). The largest relative change in seasonal mean SIA, given in percent per decade, is observed for summer: 6.13 ± 7.80 (Table 4).

3.3.2. Five longitudinal sectors

Regionally, the basic qualitative results remain largely the same for ice areas as for ice extents. The Weddell Sea has the largest magnitude of variation in monthly SIA, followed by the Ross Sea, Indian Ocean, Bellingshausen/Amundsen seas, and western Pacific Ocean (Figs. S1d–S5d). The monthly deviations of SIA are positive in the Weddell Sea, Ross Sea, and Indian Ocean and are negative in the Bellingshausen/Amundsen seas and western Pacific Ocean, with the highest magnitude slope being the positive slope for the Ross Sea and the second highest being the one for the Indian Ocean (Figs. S1e–S5e). Similar to SIE, the Weddell Sea, Ross Sea, and Indian Ocean have positive yearly changing rates of SIA; the Ross Sea has the highest one, with a yearly changing rate of $(13.16 \pm 8.87) \times 10^3 \text{ km}^2 \text{ yr}^{-1}$ (Table 4). The relative change in the annual mean regional SIA is about 5% in the Ross Sea and Indian Ocean and about -5% in the Bellingshausen/Amundsen seas.

On a seasonal basis, the signs of the SIA changing rate match those of SIE but are not consistently smaller than the SIE changing rate (Figs. S1f–S5f). There is an indication that sea ice cover in the Weddell Sea in spring has become a bit more compact ($23.93 \times 10^3 \text{ km}^2 \text{ yr}^{-1}$ for SIA instead of $16.64 \times 10^3 \text{ km}^2 \text{ yr}^{-1}$ for SIE), while in the Ross Sea there seems to be a tendency for slightly less compact ice in summer, autumn, and winter, with $8.91 \times 10^3 \text{ km}^2 \text{ yr}^{-1}$ for SIA vs. $14.51 \times 10^3 \text{ km}^2 \text{ yr}^{-1}$ for SIE in summer, $20.21 \times 10^3 \text{ km}^2 \text{ yr}^{-1}$ for SIA vs. $24.13 \times 10^3 \text{ km}^2 \text{ yr}^{-1}$ for SIE in autumn, and $9.60 \times 10^3 \text{ km}^2 \text{ yr}^{-1}$ for SIA vs. $13.89 \times 10^3 \text{ km}^2 \text{ yr}^{-1}$ for SIE in winter (Tables 3 & 4).

Table 4. As for Table 3, but for SIA. SO: Southern Ocean; WS: Weddell Sea; RS: Ross Sea; IO: Indian Ocean; BS: Bellingshausen and Amundsen seas; PO: western Pacific Ocean

	SIA		R
	($10^3 \text{ km}^2 \text{ yr}^{-1}$)	(% decade $^{-1}$)	
Yearly			
SO	17.37 ± 9.51	1.87 ± 1.03	1.83
WS	4.84 ± 9.83	1.23 ± 2.51	0.49
RS	13.16 ± 8.87	6.14 ± 4.14	1.48
IO	7.13 ± 05.08	4.91 ± 3.50	1.40
BS	-5.79 ± 4.34	-6.44 ± 4.83	-1.33
PO	-1.97 ± 3.20	-2.30 ± 3.75	-0.62
Spring			
SO	43.54 ± 15.57	3.82 ± 1.36	2.80
WS	23.93 ± 15.78	5.46 ± 3.60	1.52
RS	13.91 ± 13.21	4.96 ± 4.71	1.05
IO	11.90 ± 8.69	5.42 ± 3.96	1.37
BS	-6.95 ± 7.75	-6.21 ± 6.92	-0.90
PO	0.75 ± 4.11	0.82 ± 4.51	0.18
Summer			
SO	15.66 ± 19.94	6.13 ± 7.80	0.79
WS	5.73 ± 13.68	4.05 ± 9.68	0.42
RS	8.91 ± 10.15	20.16 ± 22.96	0.88
IO	2.86 ± 2.82	20.08 ± 19.75	1.01
BS	-0.04 ± 4.14	-0.17 ± 17.67	-0.01
PO	-1.81 ± 3.48	-5.57 ± 10.74	-0.52
Autumn			
SO	5.89 ± 22.17	0.72 ± 2.71	0.27
WS	-6.49 ± 16.99	-1.78 ± 4.65	-0.38
RS	20.21 ± 10.69	10.67 ± 5.33	1.89
IO	3.38 ± 5.86	3.83 ± 6.63	0.58
BS	-7.14 ± 7.59	-8.65 ± 9.20	-0.94
PO	-4.06 ± 4.85	-4.96 ± 5.93	-0.84
Winter			
SO	4.39 ± 11.50	0.29 ± 0.77	0.38
WS	-3.81 ± 10.98	-0.61 ± 1.76	-0.35
RS	9.60 ± 11.79	2.90 ± 3.56	0.81
IO	10.37 ± 10.91	4.02 ± 4.23	0.95
BS	-9.02 ± 7.88	-6.38 ± 5.57	-1.14
PO	-2.75 ± 6.23	-2.02 ± 4.59	-0.44

3.4. Relationships between SIC and SST

Among the algorithms mentioned in Section 2, both SICCI and OSISAF are based on the BR and BF algorithms, the SICCI algorithm is similar to the OSISAF algorithm, and only the NT algorithm is a 'real' independent algorithm. Therefore, we discuss our results based on the SICCI dataset in comparison to results from other studies based on the NT algorithm. The overall increase in sea ice over the Southern Ocean in this study, especially in the Weddell Sea, Ross Sea, and Indian Ocean, is consistent with previous studies (Cavalieri et al. 2003, Parkinson & Cavalieri 2012, Simmonds 2015). This study shows that the mean yearly SIE and SIA trends over the Southern Ocean during the period 1992–2008 are $(17.75 \pm 11.50) \times 10^3$ and $(17.37 \pm 9.51) \times 10^3 \text{ km}^2 \text{ yr}^{-1}$, respectively, while the corresponding trends during the period 1978–2010 from the study of Parkinson & Cavalieri (2012) are $(17.50 \pm 4.10) \times 10^3$ and $(15.30 \pm 3.40) \times 10^3 \text{ km}^2 \text{ yr}^{-1}$, respectively (Table 5). This indicates that the trends from both studies are not significantly different from each other. The trend of a shorter period under the umbrella of a longer period can help us to understand the more detailed structure of a long-term trend and non-uniformity within a long-term period since the variation of sea ice with time may not be uniform. The case that the western Pacific Ocean has a negative trend in sea ice cover for the shorter period of 1992–2008 but a positive one for the longer period of 1979–2013 is a good example. The implications of this for our current and future understanding of Antarctic sea ice cover changes is that the trend of the shorter period of recent or future events under the umbrella of a long period of time should also be investigated since the more recent trend may have more weight in the prediction of sea ice status than just the long-term trend.

Regionally, the mean yearly SIE and SIA trends in the Weddell Sea, Ross Sea, Indian Ocean, and Bel-

Table 5. Comparisons between yearly sea ice extent (SIE) and sea ice area (SIA) changing rates (\pm SDs) in this study and corresponding changing rates from the study of Parkinson & Cavalieri (2012) in the Southern Ocean as a whole and in the 5 longitudinal sectors (units: $10^3 \text{ km}^2 \text{ yr}^{-1}$). SICCI: Sea Ice Climate Change Initiative; SO: Southern Ocean; WS: Weddell Sea; RS: Ross Sea; IO: Indian Ocean; BS: Bellingshausen and Amundsen seas; PO: western Pacific Ocean

Parameter	Time period	Algorithm	Location					
			SO	WS	RS	IO	BS	PO
SIE	1992–2008	SICCI	17.75 ± 11.50	2.05 ± 11.95	16.68 ± 10.49	8.98 ± 4.99	-8.45 ± 10.65	-2.93 ± 3.94
SIE	1979–2010	NASA Team	17.50 ± 4.10	5.20 ± 4.50	13.70 ± 3.60	5.90 ± 2.20	-7.80 ± 2.50	0.60 ± 1.80
SIA	1992–2008	SICCI	17.37 ± 9.51	4.84 ± 9.83	13.16 ± 8.87	7.13 ± 5.08	-5.79 ± 4.34	-1.97 ± 3.20
SIA	1979–2010	NASA Team	15.30 ± 3.40	4.40 ± 3.60	10.90 ± 2.90	4.20 ± 2.00	-5.60 ± 1.90	1.40 ± 1.30

lingshausen and Amundsen seas from both studies are also not significantly different from each other (Table 5). This study confirms the previous findings that sea ice in the whole Southern Ocean, Weddell Sea, Ross Sea, and Indian Ocean increased, while sea ice in the Bellingshausen and Amundsen seas decreased during these periods. However, the mean yearly SIE and SIA trends in the western Pacific Ocean from both studies are different. Although the trends are consistent in winter, they are different in all of the other 3 seasons, which results in the inconsistency. This fact indicates that sea ice change in the western Pacific Ocean is worth further investigation.

SST plays an important role in sea ice changes. A decreasing SST is beneficial to sea ice production, resulting in an increase in sea ice coverage, and vice versa. During the 17 yr period, SST fluctuated, with a slight cooling changing rate in the Southern Ocean as well as in the 5 sectors except for the Bellingshausen/Amundsen seas (Fig. 5), although their changing rates are not significant. Yearly SIE and SIA are significantly negatively correlated with yearly SST in the Southern Ocean, and each of the 5 sectors (Fig. 6) at the significance level above 95% (Tables 6 & 7). Negative correlation between SIE and temperature in Antarctica is also found by Shu et al. (2012). The negative correlations indicate that the decreases in SST resulted in sea ice increases in the Weddell Sea, Ross Sea, and Indian Ocean and that an increase in SST resulted in sea ice decreases in the Bellingshausen/Amundsen seas, and these were verified by Vaughan et al. (2003).

During the 4 seasons, SIEs in the Southern Ocean or each of the 5 sectors are also significantly negatively correlated with the corresponding SST, except for the Weddell Sea in winter (Tables 6 & 7), and correlation coefficients in spring and autumn are much higher than those in winter and summer. This suggests that sea ice is more sensitive to SST in spring and autumn when melting/lateral decay or growth of sea ice may be more pronounced than that in summer and winter, since sea ice formation and melting are closely correlated to SST variation around -1.8°C .

However, there is an exception in the western Pacific Ocean (Tables 6 & 7). Although the relationships between SST and SIE or SIA are significant, the decrease in SST did not result in an increase in sea ice; instead, sea ice decreased. This may indicate that in the western Pacific Ocean, SST may not be a dominant factor in sea ice growth or decay and that other factors such as wind or ocean currents may play a predominant role. Holland & Kwok (2012) pointed out that wind-driven changes in ice advection are the

dominant driver of a slight increase in Antarctic sea ice. Observations and atmospheric reanalysis show that Antarctic sea ice changes are linked to intensified meridional winds on multidecadal time scales (Haumann et al. 2014). A comprehensive set of ocean–sea ice simulations also shows that wind variability is an important determinant of the heterogeneous pattern of the variability and trends of sea ice in the Southern Ocean (Matear et al. 2015).

4. CONCLUSIONS

The SSM/I SIC data based on the ESA SICCI algorithm are assessed and used in this study, which is based on a more recent time series of SICs between 1992 and 2008. We investigate whether the SICCI dataset is equally suitable for studying sea ice cover changes in the Southern Ocean as other datasets. We then examine spatiotemporal variations in sea ice derived from the SICCI dataset over the Southern Ocean and analyse sea ice relationships with SST. The results indicate that the SICCI dataset is on a par with the NT dataset, and can therefore be used for studying sea ice changes. The 2 datasets are not significantly different from each other, and show that the overall sea ice over the Southern Ocean has a slight positive trend. This study confirms the previous findings that sea ice in the whole Southern Ocean, Weddell Sea, Ross Sea, and Indian Ocean increased, while sea ice in the Bellingshausen and Amundsen seas decreased during the 1992–2008 (this study) and 1978–2010 (Parkinson & Cavalieri 2012) periods. Antarctic sea ice has significant seasonal variations; all seasonally averaged SIE and SIA show positive changing rates, with spring showing the largest positive changing rates followed by summer. The Weddell Sea, Ross Sea, and Indian Ocean have positive yearly changing rates of SIE and SIA, and make important contributions to the increase in sea ice over the Southern Ocean because of their large sea ice cover or positive yearly changing rates. However, the Bellingshausen/Amundsen seas and western Pacific Ocean have negative yearly changing rates. Although sea ice in the Bellingshausen/Amundsen seas and western Pacific Ocean decreased, there was no evident effect on the overall sea ice change in the Southern Ocean as a whole because these areas have small sea ice cover and proportions in total.

We calculated the monthly mean SST of pixels for which the corresponding SICs are $>15\%$ for the 5 longitudinal sectors and the Southern Ocean, and

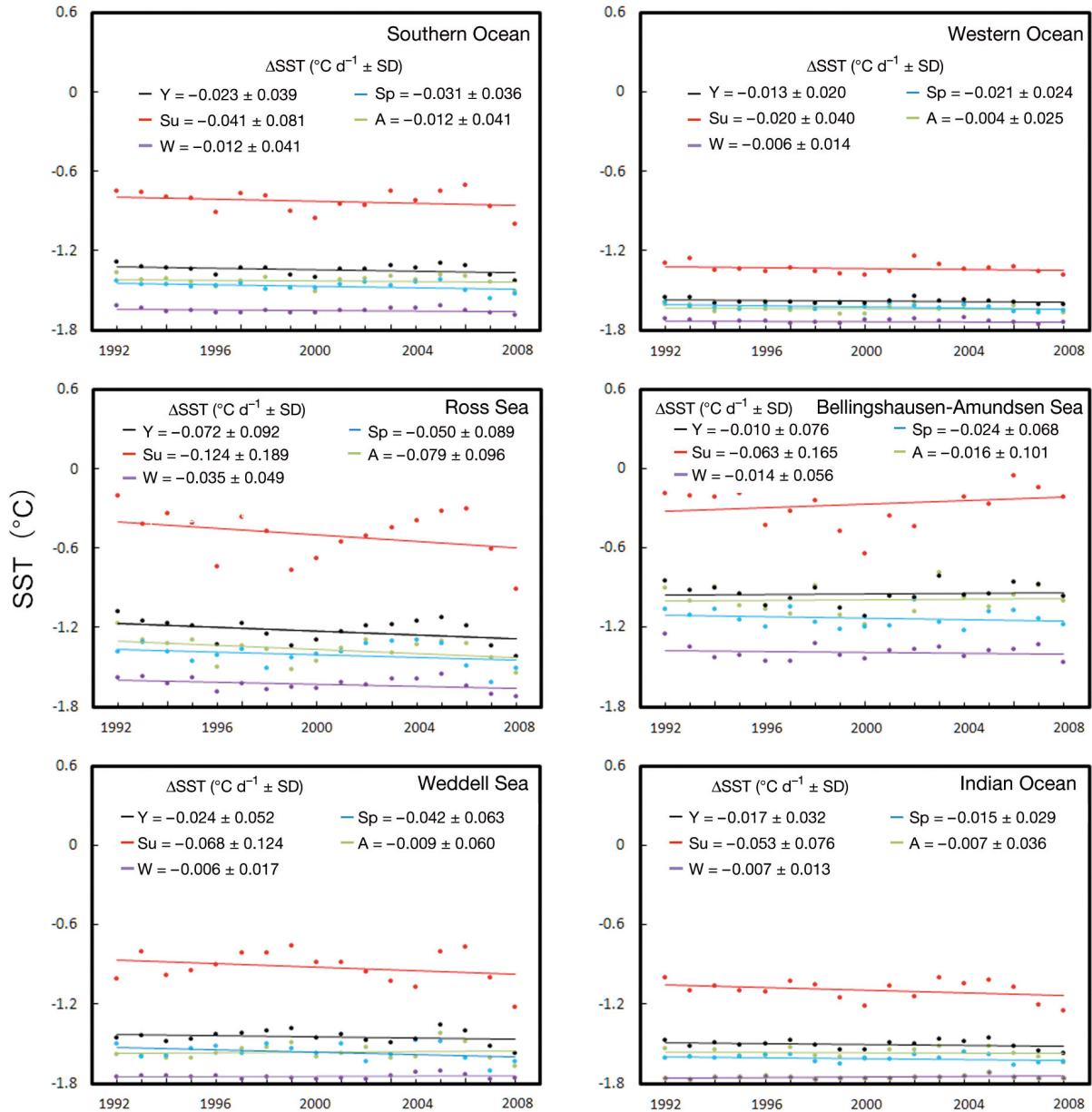


Fig. 5. Time series of yearly and seasonal sea surface temperatures for the Southern Ocean as a whole and for the 5 longitudinal sectors from January 1992 to December 2008. Y: yearly averages; Su: summer averages (January–March); A: autumn averages (April–June); W: winter averages (July–September); Sp: spring averages (October–December)

established the corresponding monthly SST time series. Both SIE and SIA are significantly negatively correlated with SST in the Southern Ocean and each of the 5 sectors, and sea ice is more sensitive to SST in spring and autumn. A decrease (increase) in SST is associated with the increase (decrease) in SIE and SIA, and the decrease in SST is one of the main reasons for the sea ice increase in the Southern Ocean from 1992 to 2008. Besides SST or surface air temperature, other forcings such as ocean currents, wind (Baba et al. 2006, Holland & Kwok 2012, Haumann et

al. 2014, Matear et al. 2015), the El Niño-Southern Oscillation (ENSO) (Stammerjohn et al. 2012), and the Southern Annular Mode (Comiso et al. 2011, Pezza et al. 2012) may also play an important role in Antarctic sea ice change, and they will be examined in the future.

Sea ice change can be measured not only by its concentration, extent, and area but also by thickness, which is not studied in this paper. Variations of sea ice thickness will be explored with the release of improved products of sea ice thickness in the ESA

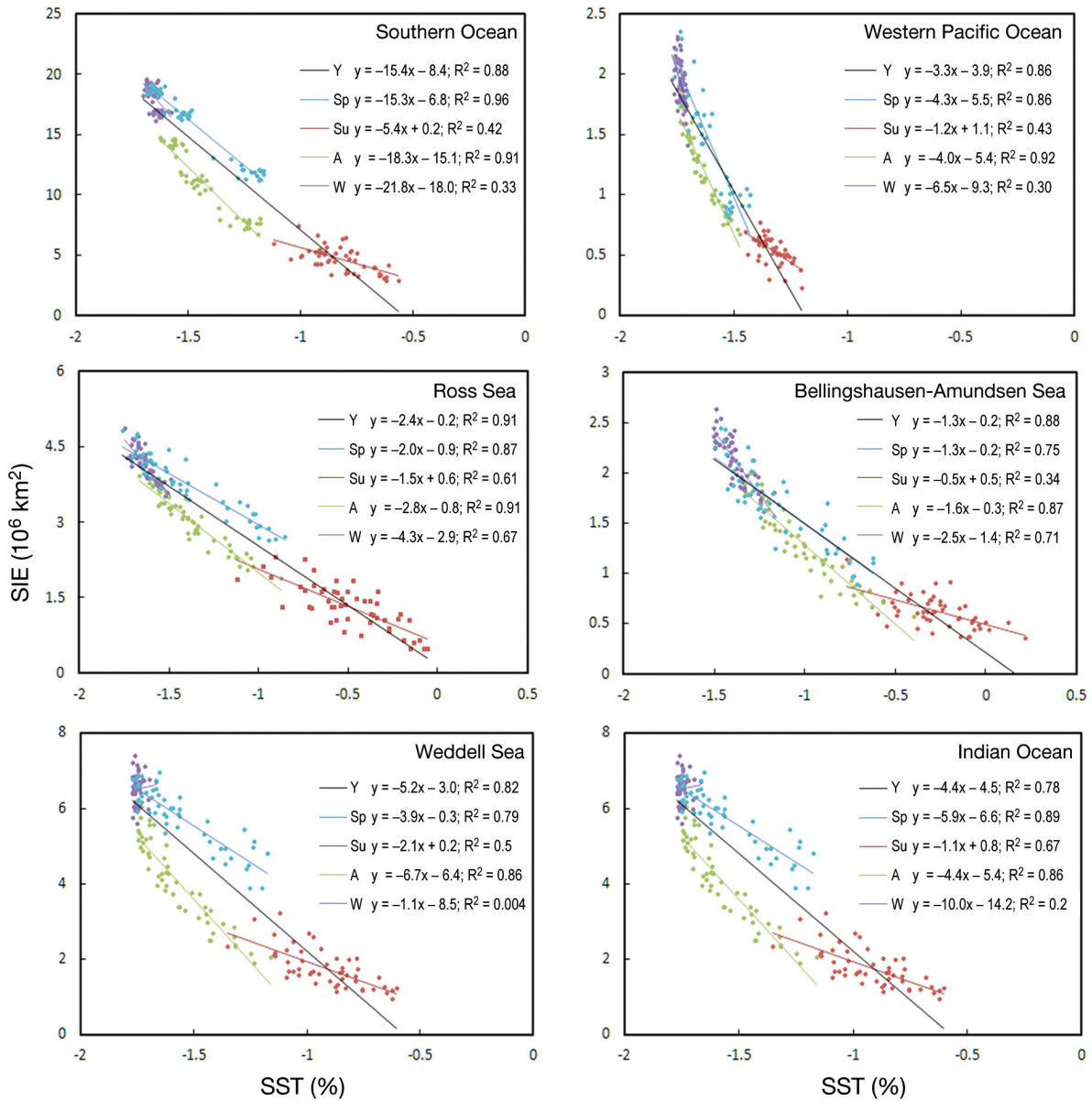


Fig. 6. Relationships between yearly and seasonal sea ice extents and corresponding sea surface temperatures for the Southern Ocean as a whole and for the 5 longitudinal sectors from January 1992 to December 2008. Y: yearly averages; Su: summer averages (January–March); A: autumn averages (April–June); W: winter averages (July–September); Sp: spring averages (October–December)

Table 6. Correlation coefficients between sea ice extents and sea surface temperatures; **bold** indicates statistical significance of $\geq 95\%$. SO: Southern Ocean; WS: Weddell Sea; RS: Ross Sea; IO: Indian Ocean; BS: Bellingshausen and Amundsen seas; PO: western Pacific Ocean

Time scale	SO	WS	RS	IO	BS	PO
Yearly	-0.94	-0.90	-0.95	-0.89	-0.94	-0.93
Spring	-0.98	-0.89	-0.93	-0.94	-0.87	-0.92
Summer	-0.65	-0.71	-0.78	-0.82	-0.59	-0.65
Autumn	-0.95	-0.93	-0.96	-0.93	-0.93	-0.96
Winter	-0.58	0.06	-0.82	-0.44	-0.84	-0.55

Table 7. Same as Table 4 but for SIA. SO: Southern Ocean; WS: Weddell Sea; RS: Ross Sea; IO: Indian Ocean; BS: Bellingshausen and Amundsen seas; PO: western Pacific Ocean

Time scale	SO	WS	RS	IO	BS	PO
Yearly	-0.95	-0.92	-0.97	-0.88	-0.94	-0.93
Spring	-0.98	-0.95	-0.97	-0.96	-0.91	-0.95
Summer	-0.64	-0.79	-0.78	-0.74	-0.46	-0.59
Autumn	-0.96	-0.93	-0.96	-0.94	-0.93	-0.96
Winter	-0.62	0.02	-0.86	-0.48	-0.83	-0.61

SICCI dataset. Additionally, with the increasing amount of optical remote sensing data, active and passive remote sensing data and satellite altimeter data, the extension of data series time spans, and the development of oceanic and atmospheric models, changes in Antarctic sea ice can be studied more comprehensively and systematically. It is thus expected that an improvement in future forecasting and analysis of the variation and trends of Antarctic sea ice can be achieved by combining multisource remote sensing data with numerical models.

Acknowledgements. This work was financially supported by the Program for National Nature Science Foundation of China (No.41371391, No.J1210015), the National Key Research and Development Program (2016YFA0600102), and the Program for Foreign Cooperation of Chinese Arctic and Antarctic Administration (No. IC201301). The SICCI sea ice concentration products used in this study were downloaded from the website <http://icdc.zmaw.de>. We thank the 2 anonymous reviewers and the editor for valuable comments and suggestions that greatly improved the quality of this paper.

LITERATURE CITED

- Andersen S, Tonboe R, Kern S, Schyberg H (2006) Improved retrieval of sea ice total concentration from spaceborne passive microwave observations using numerical weather prediction model fields: an intercomparison of nine algorithms. *Remote Sens Environ* 104:374–392
- Baba K, Minobe S, Kimura N, Wakatsuchi M (2006) Intra-seasonal variability of sea-ice concentration in the Antarctic with particular emphasis on wind effect. *J Geophys Res* 111:C12023
- Cavalieri DJ, Parkinson CL (2012) Arctic sea ice variability and trends, 1979–2010. *Cryosphere* 6:957–979
- Cavalieri DJ, Gloersen P, Campbell WJ (1984) Determination of sea ice parameters with the NIMBUS 7 SMMR. *J Geophys Res* 89:5355–5369
- Cavalieri DJ, Parkinson CL, Gloersen P, Comiso JC, Zwally HJ (1999) Deriving long-term time series of sea ice cover from satellite passive-microwave multisensor data sets. *J Geophys Res* 104:15803–15814
- Cavalieri DJ, Parkinson CL, Vinnikov KY (2003) 30-year satellite record reveals contrasting Arctic and Antarctic decadal sea ice variability. *Geophys Res Lett* 30:1970
- Comiso JC (1986) Characteristics of Arctic winter sea ice from satellite multispectral microwave observations. *J Geophys Res* 91:975–994
- Comiso JC (2010) *Polar oceans from space*. Springer, New York, NY
- Comiso JC, Nishio F (2008) Trends in the sea ice cover using enhanced and compatible AMSR-E, SSM/I, and SMMR data. *J Geophys Res* 113:C02S07
- Comiso JC, Cavalieri DJ, Parkinson LC, Gloersen P (1997) Passive microwave algorithms for sea ice concentration: a comparison of two techniques. *Remote Sens Environ* 60:357–384
- Comiso JC, Kwok R, Martin S, Gordon AL (2011) Variability and trends in sea ice extent and ice production in the Ross Sea. *J Geophys Res* 116: C04021
- Eastwood S (ed) (2012) *Ocean & sea ice SAF, sea ice product manual*, version 3.8. <http://osisaf.met.no> (accessed March 8, 2015)
- Gallaher DW, Campbell GG, Meier WN (2014) Anomalous variability in Antarctic sea ice extents during the 1960s with the use of Nimbus data. *IEEE J Sel Top Appl Earth Obs Remote Sens* 6:1116–1122
- Goosse H, Zunz V (2014) Decadal trends in the Antarctic sea ice extent ultimately controlled by ice–ocean feedback. *Cryosphere* 8:453–470
- Hanna E (1996) The role of Antarctic sea ice in global climate change. *Prog Phys Geogr* 20:371–401
- Haumann FA, Notz D, Schmidt H (2014) Anthropogenic influence on recent circulation-driven Antarctic sea ice changes. *Geophys Res Lett* 41:8429–8437
- Holland PR (2014) The seasonality of Antarctic sea ice trends. *Geophys Res Lett* 41:4230–4237
- Holland PR, Kwok R (2012) Wind-driven trends in Antarctic sea ice drift. *Nat Geosci* 5:872–875
- Hollinger J, Lo R, Poe G, Savage R, Peirce J (1987) *Special Sensor Microwave/Imager user's guide*. Naval Research Laboratory, Washington, DC
- Ivanova N, Pedersen LT, Tonboe RT, Kern S and others (2015) Inter-comparison and evaluation of sea ice algorithms: towards further identification of challenges and optimal approach using passive microwave observations. *Cryosphere* 9:1797–1817
- Kaleschke L, Lupkes C, Vihma T, Haarpaintner J, Bochert A, Hartmann J, Heygster G (2001) SSM/I sea ice remote sensing for mesoscale ocean–atmosphere interaction analysis. *Can J Rem Sens* 27:526–537
- Matear RJ, O’Kane TJ, Risbey JS, Chamberlain M (2015) Sources of heterogeneous variability and trends in Antarctic sea-ice. *Nat Commun* 6:8656
- Parkinson CL, Cavalieri DJ (2012) Antarctic sea ice variability and trends, 1979–2010. *Cryosphere* 6:871–880
- Pezza AB, Rashid HA, Simmonds I (2012) Climate links and recent extremes in Antarctic sea ice, high-latitude cyclones, Southern Annular Mode and ENSO. *Clim Dyn* 38:57–73
- Raphael MN, Hobbs W (2014) The influence of the large-scale atmospheric circulation on Antarctic sea ice during ice advance and retreat seasons. *Geophys Res Lett* 41: 5037–5045
- Raphael MN, Hobbs W, Wainer I (2011) The effect of Antarctic sea ice on the Southern Hemisphere atmosphere during the southern summer. *Clim Dyn* 36:1403–1417
- Reynolds RW, Rayner NA, Smith TM, Stokes DC, Wang W (2002) An improved in situ and satellite SST analysis for climate. *J Clim* 15:1609–1625
- Shao ZD, Ke CQ (2015) Spring–summer albedo variations of Antarctic sea ice from 1982 to 2009. *Environ Res Lett* 10: 064001
- Shu Q, Qiao F, Song Z, Wang C (2012) Sea ice trends in the Antarctic and their relationship to surface air temperature during 1979–2009. *Clim Dyn* 38:2355–2363
- Simmonds I (2015) Comparing and contrasting the behaviour of Arctic and Antarctic sea ice over the 35 year period 1979–2013. *Ann Glaciol* 56:18–28
- Simpkins GR, Ciasto LM, England MH (2013) Observed variations in multidecadal Antarctic sea ice trends during 1979–2012. *Geophys Res Lett* 40:3643–3648
- Smith DM (1996) Extraction of winter total sea-ice concen-

- tration in the Greenland and Barents seas from SSM/I data. *Int J Remote Sens* 17:2625–2646
- ✦ Spreen G, Kaleschke L, Heygster G (2008) Sea ice remote sensing using AMSR-E 89-GHz channels. *J Geophys Res* 113:C02S03
- ✦ Stammerjohn S, Massom R, Rind D, Martinson D (2012) Regions of rapid sea ice change: an interhemispheric seasonal comparison. *Geophys Res Lett* 39:L06501
- ✦ Svendsen E, Kloster K, Farrelly B, Johannessen OM and others (1983) Norwegian remote sensing experiment evaluation of the Nimbus 7 scanning multichannel microwave radiometer for sea ice research. *J Geophys Res* 88:2781–2791
- Taylor JR (ed) (1997) Least-squares fitting. In: *An introduction to error analysis: the study of uncertainties in physical measurements*, 2nd edn. University Science Books, Sausalito, CA, p 181–207
- ✦ Vaughan DG, Marshall GJ, Connolley WM, Parkinson C and others (2003) Recent rapid regional climate warming on the Antarctic Peninsula. *Clim Change* 60:243–274
- Vaughan DG, Comiso JC, Allison I, Carrasco J and others (2013) Observations: cryosphere. In: Stocker TF, Qin D, Plattner GK, Tignor M and others (eds) *Climate change 2013: the physical science basis. Contribution of working group I to the fifth assessment report of the Intergovernmental Panel on Climate Change*. Cambridge University Press, Cambridge, p 317–382
- ✦ Walsh JE, Chapman WL (2001) 20th-century sea-ice variations from observational data. *Ann Glaciol* 33:444–448
- ✦ Worby AP, Comiso JC (2004) Studies of the Antarctic sea ice edge and ice extent from satellite and ship observations. *Remote Sens Environ* 92:98–111
- ✦ Yuan X, Martinson DG (2000) Antarctic sea ice extent variability and its global connectivity. *J Clim* 13: 1697–1717
- ✦ Zhou X, Li S, Morris K, Jeffries MO (2007) Albedo of summer snow on sea ice, Ross Sea, Antarctica. *J Geophys Res* 112:D16105

Editorial responsibility: Nils Chr. Stenseth, Oslo, Norway

*Submitted: August 17, 2015; Accepted: October 10, 2016
Proofs received from author(s): December 22, 2016*